Manipulation of a Round Jet with Electromagnetic Flap Actuators

Hiroaki Suzuki, Nobuhide Kasagi, Yuji Suzuki, and Hiroki Shima
Department of Mechanical Engineering
The University of Tokyo
7-3-1, Hongo, Bunkyo-ku, Tokyo 113-8656, Japan
e-mail: kasagi@thtlab.t.u-tokyo.ac.jp

ABSTRACT

A novel axisymmetric jet nozzle equipped with a row of miniature electromagnetic flap actuators on its circular lip is developed for active flow control. Each of the flaps fabricated by photolithography is independently driven according to a control signal supplied by a PC. The spatio-temporal flow structures of the controlled jet are studied through flow visualization and laser Doppler velocimetry (LDV) measurement. It is found that artificial disturbances generated by the flaps can modify the formation and evolution of large scale vortical structures significantly. When each half cluster of these flaps are driven out of phase, the jet clearly bifurcates into two branches and its mixing is markedly enhanced in the plane of bifurcation.

INTRODUCTION

Control of shear flow and associated scalar transport has been one of the central issues in modern scientific, engineering and environmental research efforts. Its potential benefits can be easily identified if one thinks about the significance of the artificial manipulation of flow drag, noise, heat transfer as well as chemical reaction. The scales of real flow phenomena, however, are very small, typically on the order of microns, and their lifetime is also very short. In the past, direct manipulation of these scales was very difficult, but is now expected to become possible with miniature sensors and actuators fabricated by MEMS. In addition, micromechanical components will possibly be produced in large quantities through a batch production process. Thus, efforts are now directed toward to active or interactive control methodologies, particularly those exploiting emerging MEMS technology [1].

A MEMS controller unit, with its integrated mechanical parts and IC, will be able to sense the physical world, process the information, and then manipulate the physical phenomena with actuators. From this viewpoint, various studies of active flow control have been triggered. Large-scale numerical simulation has been carried out in order to test proposed control algorithms such as active cancelation, optimal control theory and neural networks [2, 3]. Some prototype tests of turbulence control have been reported; Liu et al. [4] developed a sophisticated flap actuator for the delta-wing control, in which the micro actuation is amplified to macro effect. Smith & Glezer [5] successfully applied miniature zero-mass-flux jet actuators to a macro scale planer jet for its vectorization. Huang et al. [6] developed an axisymmetric jet nozzle equipped with electrostatic micro actuators to suppress the screech in a high speed jet.

Among various shear flows, jets are used in a variety of industrial applications such as mixing, cooling/heating, drying, spraying, printing, and thrusting. In this particular flow mode, the evolution of large coherent vortical structures in the jet shear layer plays a primary role in the turbulent momentum and scalar transport. Since these structures are known to be very sensitive to the initial shear layer condition, a large alternation in the downstream flow field can be expected with a relatively small control input. Actually, this has been demonstrated by previous investigations; *e.g.*, Bradbury & Khadem [7] found that the jet flow is strongly distorted by introducing small tabs on the nozzle perimeter, while Lee & Reynolds [8] reported that a jet flow can be forced to bloom or bifurcate by a combined effect of a precessing nozzle and axial forcing.

In the present study, we pursue a possibility of producing various jet flow modes with a single axisymmetric nozzle. The fabricated nozzle is equipped with miniature actuators driven by a control program code on a PC. A key aspect is that the control power input by these actuators would be by an order of magnitude smaller than the resultant effect or output, if the chaotic nature inherent in the fluid dynamics is successfully exploited. For this purpose, electromagnetic flap actuators, of which size is on the order of millimeter, are photofabricated from a copper plated polyimide film. The spatio-temporal structure and the velocity distribution of the controlled jet are examined by flow visualization and LDV measurement, respectively.

ELECTROMAGNETIC FLAP ACTUATOR

Design of Actuator

An electromagnetic flap actuator of 9 mm in length and 3 mm in width (Fig. 1) is made of a 25 μm thick polyimide film, on which a 35 μm thick copper square coil is formed with ferric chloride etching. The flap is elastically bent by the electromagnetic force between the copper coil and a cylindrical permanent magnet of 4000 Gauss placed underneath. At the root of the

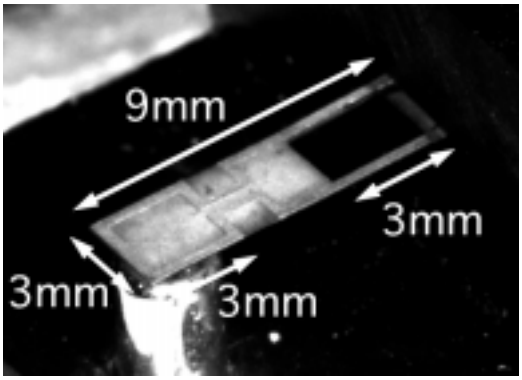

Fig. 1 Electromagnetic flap actuator.

flap, a part of the polyimide film is hollowed with a laser machining system to reduce the bending stiffness.

The potential energy between the rectangular coil and the permanent magnet Φ is expressed as a sum of the products of the magnetic moment m and the magnetic field intensity H at their positions, *i.e.*,

$$\Phi = -\frac{1}{2}(m_m H_m + m_c H_c), \qquad (1)$$

where the subscripts m and c denote the magnet and the coil, respectively. The electromagnetic force F is then derived as:

$$F(\Delta y) = \frac{\partial \Phi}{\partial(\Delta y)}, \qquad (2)$$

where Δy is the distance between the flap and the magnet. The magnetic moment of the square coil having a side length of a is given as:

$$m_c = \mu_0 i a^2, \qquad (3)$$

where μ_0 and i are the space permeability and the electric current, respectively. The magnetic moment of the permanent magnet is given with the magnetization M_m and its volume as:

$$m_m = M_m \cdot (\pi b^2 h), \qquad (4)$$

where b is the radius and h is the height of the cylindrical magnet. The quantity M_m can be estimated from the surface magnetic flux density. The magnetic field intensities H_c and H_m are given by the Biot-Savart's law, while H_c at the center of the coil induced by the magnet is calculated with an assumption that the magnet works as a solenoid of the same volume and the same surface magnetic flux density.

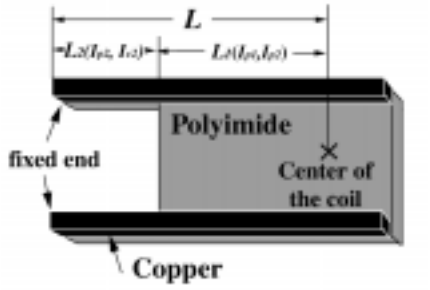

Fig. 2 Composite beam model.

The static and dynamic response of the flap are calculated by using a composite beam model as shown in Fig. 2. The distance between the fixed end to the center of the coil is defined as L, while the lengths of the flat plate and the supporting beam are denoted as L_1 and L_2, respectively. The copper layer is modelled as two straight bars. With this model, the static deflection y is given as:

$$y = \frac{1}{3}\left(\frac{L^3 - L_1^3}{(E_p I_{p2} + E_c I_{c2})} + \frac{L_1^3}{(E_p I_{p1} + E_c I_{c1})}\right)F, \qquad (5)$$

where E_p (= 3.0×10^9 N/m^2) and E_c (= 12.98×10^{10} N/m^2) are respectively the Young's moduli of polyimide and copper, while I is the moment of inertia of each section. The resonant frequency f_{res} is given as:

$$f_{res} = \frac{1}{2\pi}\frac{\lambda^2}{L^2}\sqrt{\frac{E_p I_p + E_c I_c}{\rho_p A_p + \rho_c A_c}}, \qquad (6)$$

where λ (= 1.875) is the vibration coefficient, and ρ_p (= 1.42×10^3 kg/m^3) and ρ_c (= 8.96×10^3 kg/m^3) are the density of polyimide and that of copper, respectively.

Static and Dynamic Responses of Actuator

The displacement of the flap, which is measured at the center of the coil by using a laser displacement meter (Keyence; LC-2440), is shown in Fig. 3. In this measurement, the original position of the flap is in contact with the top of the magnet; this is the same arrangement as in the case of the jet nozzle described later. The flap is capable of achieving about 0.4 mm displacement with a DC 1 A and exhibits an almost linear response to direct current. However, its gradient gradually decreases at higher current, due to the larger distance between the coil and magnet. The prediction of the flap displacement derived from Eqs. (2) and (5) is in good agreement with the measurement data.

Figure 4 shows the frequency response of the flap with an AC 0.8 A. In this case, the flap is placed one millimeter above the magnet to avoid the flap from hitting the top of the magnet. The first resonant frequency in air is 270 Hz with the peak-to-peak displacement of about 1.6 mm. The resonant frequency predicted by Eq. (6) is 276 Hz, which is also in good agreement with the measured value.

In water, the resonant frequency is much reduced due to the reactive fluid forces; it drops to 60 Hz. To examine this change, the composite beam model is further simplified to a lumped parameter system, which consists of mass m, spring k, and viscous dumper c as:

$$m\ddot{y} + c\dot{y} + ky = F - F_R, \qquad (7)$$

where F and F_R are the electromagnetic and fluid forces, respectively. By choosing appropriate values of m, c and k, and

neglecting F_R, the frequency response of the flap in air can be reasonably well predicted as shown in Fig. 4. In the case of the flap in water, the fluid force F_R is estimated from separate numerical simulation of an unsteady flow around a flapping plate in stationary fluid, *i.e.*, F_R is found to be proportional to the square of its velocity, *i.e.*, $r|\dot{y}|\dot{y}$. The predicted response of the lumped system in water is also shown in Fig. 4, where it does not coincide well with the measured data. This discrepancy should be partially due to the assumption that the flap is rigid, but not flexible, so that a more sophisticated flap model should be developed. Further numerical analysis is now undertaken to examine the fluid force acting on the flap under more realistic conditions.

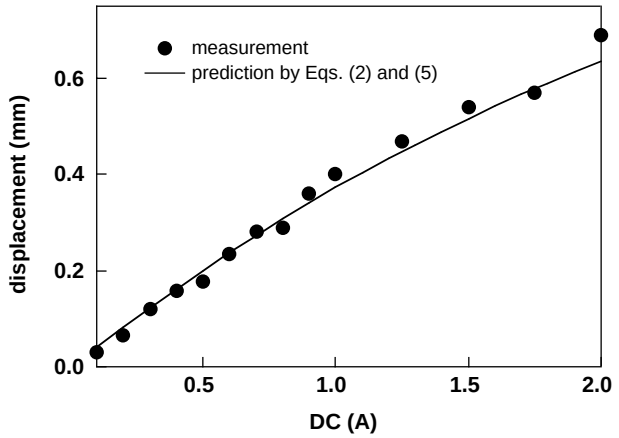

Fig. 3 Static response of the flap.

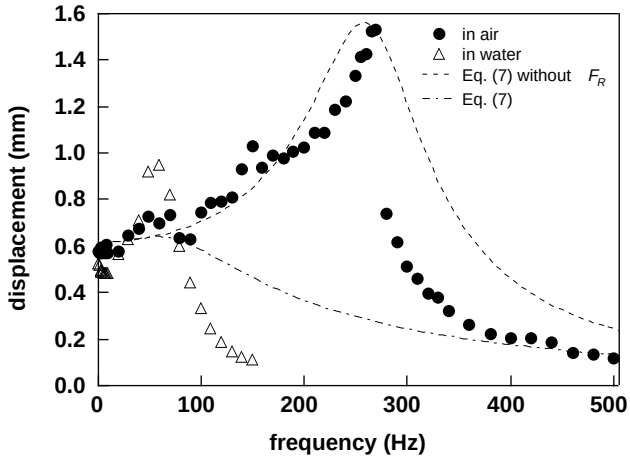

Fig. 4 Frequency response of the flap.

EXPERIMENTAL FACILITY AND PROCEDURE

Figure 5 shows a perspective view of the fabricated jet nozzle (diameter D = 20mm) with 18 flap actuators on its exit lip. These flaps placed at even intervals cover 86% of the circumference. Each flap is driven independently by the amplified signal from a multi-channel digital-analog board. A schematic of the water tank facility is depicted in Fig. 6. The jet nozzle and a plenum are connected horizontally. Water is driven by a magnetic pump through a honeycomb and meshes in the 130 mm ID plenum in order to reduce the fluctuation and obtain a uniform mean flow distribution at the nozzle exit. The nozzle has an area contraction ratio of 42 : 1. The jet is discharged horizontally into a water tank of 900 mm in length, 800 mm in width, and 800 mm in height. The bulk flow rate is measured by a turbine flowmeter (AATEC; IR-OPFLOW) installed upstream of the plenum. Axial forcing, which is a conventional method to control the vortex shedding, is achieved by oscillating a 20 mm diameter circular disk located upstream of the plenum with a voice coil motor.

To examine qualitatively the global behavior of large scale structures and entrainment/mixing characteristics of the jet flow, the jet shear layer is visualized with fluorescent dye (Rhodamine B) injected from an annular slot of one millimeter in width assembled inside the nozzle. A 20 mJ YAG pulse laser (Newwave Research; Mini Lase II) sheet and a stroboscope are employed for illumination of sectional and perspective views, respectively. These images are acquired by a 3 CCD color camera (Sony; XC-003) and recorded onto a laser disk recorder (Sony; LVR-5000). To measure the transverse and longitudinal velocity components in the jet flow, a two-component fiber LDV (DANTEC; 60X11) is employed.

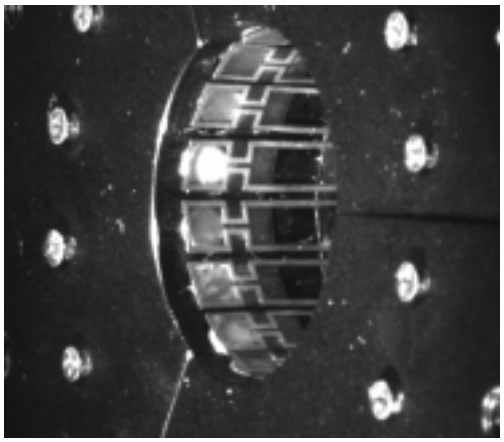

Fig. 5 Perspective view of the nozzle exit with 18 flap actuators.

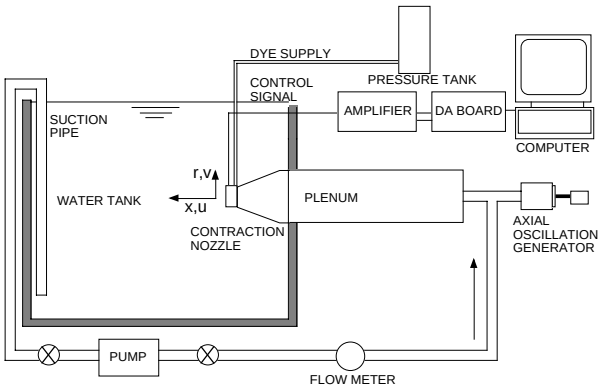

Fig. 6 Recirculating water jet facility.

RESULTS

Flow Visualization

In the flow visualization experiment, the bulk flow rate U_b is kept at 118 mm/s, and the resultant Reynolds number, U_bD/ν, is 2500. A typical longitudinal sectional view of a natural jet is shown in Fig. 7. A laminar shear layer roles up into discrete vortex rings at about x/D = 2.

Figure 8 shows a longitudinal cross sectional view of the jet controlled by the axisymmetric flap motion, in which all 18 flaps are driven synchronously by a square wave signal of f = 4Hz. This corresponds to the dimensionless Strauhal number defined as $St_a = fD/U_b$ of 0.675. Axisymmetric vortex rings with a regular spacing are formed. Thus, the roll-up and the shedding of coherent vortical structures can be synchronized with the flap movement as has been observed in the experiments with speakers and diaphragms [9].

When the jet is excited with spiral movement of the flaps at 1.6 Hz (St_a = 0.27) combined with the axial forcing at 3.2 Hz, the vortex rings are inclined and alternatively displaced off the jet axis as shown in Fig. 9. In this case, sinuous movement of each adjacent flap is deferred by 20 degree in phase. The eccentric vortices induce each other a radial velocity component to deviate from the jet axis as they are convected downstream and then divided into two branches around x/D=5. This phenomenon is in accordance with the observation by Lee & Reynolds [8].

When upper and lower halves of the 18 flaps are driven out of phase with square wave signals (hereafter, Alternative Mode) at 1.6 Hz (St_a = 0.27), the jet bifurcates into two branches more clearly as shown in Fig. 10. In this case, alternatively inclined

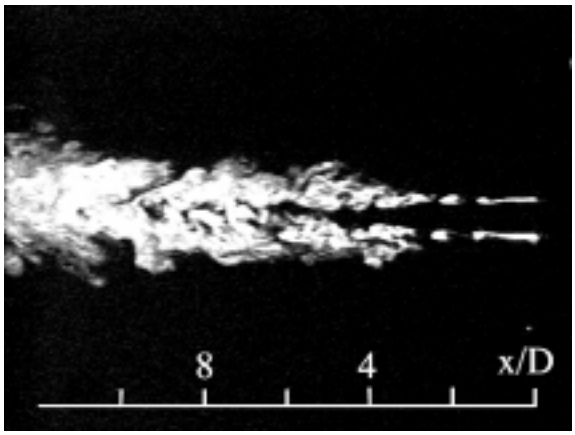

Fig. 7 Longitudinal sectional view of natural jet.

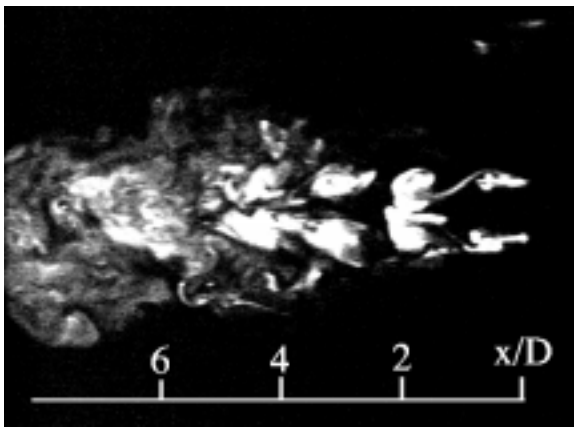

Fig. 8 Axisymmetric structures locked in synchronous flap movement at 4 Hz.

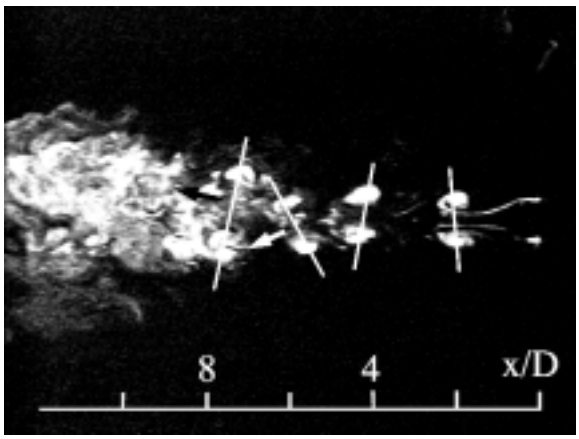

Fig. 9 Bifurcating jet generated by spiral flap movement at 1.6 Hz combined with axial forcing at 3.2 Hz.

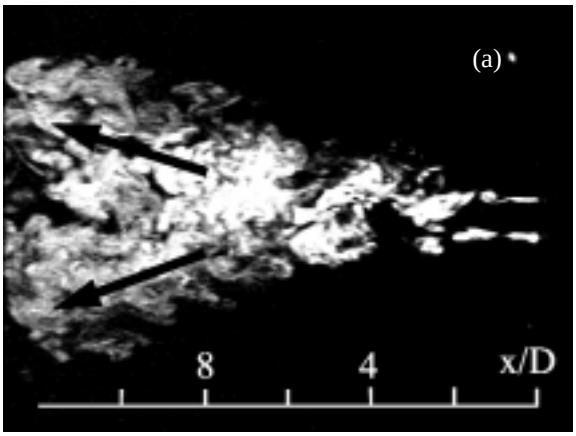

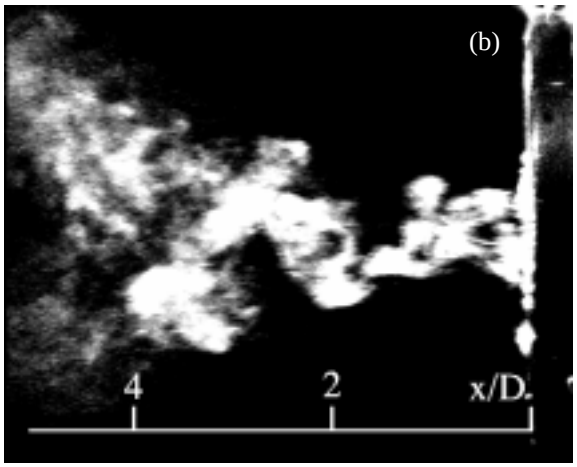

Fig. 10 (a) Bifurcating jet excited with two halves of flaps out of phase (Alternalive Mode) at 1.6Hz,
(b) Close-up view.

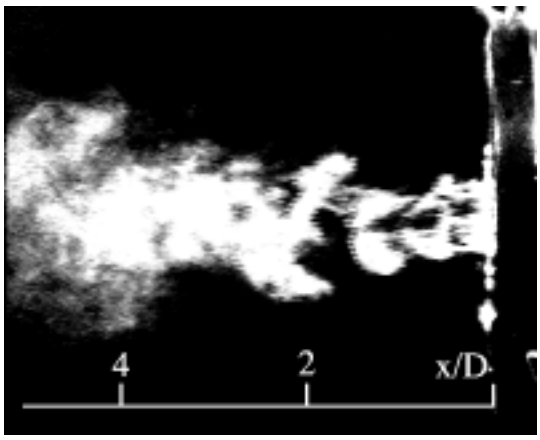

Fig. 11 Jet furcating into six directions in Rotary Alternative Mode.

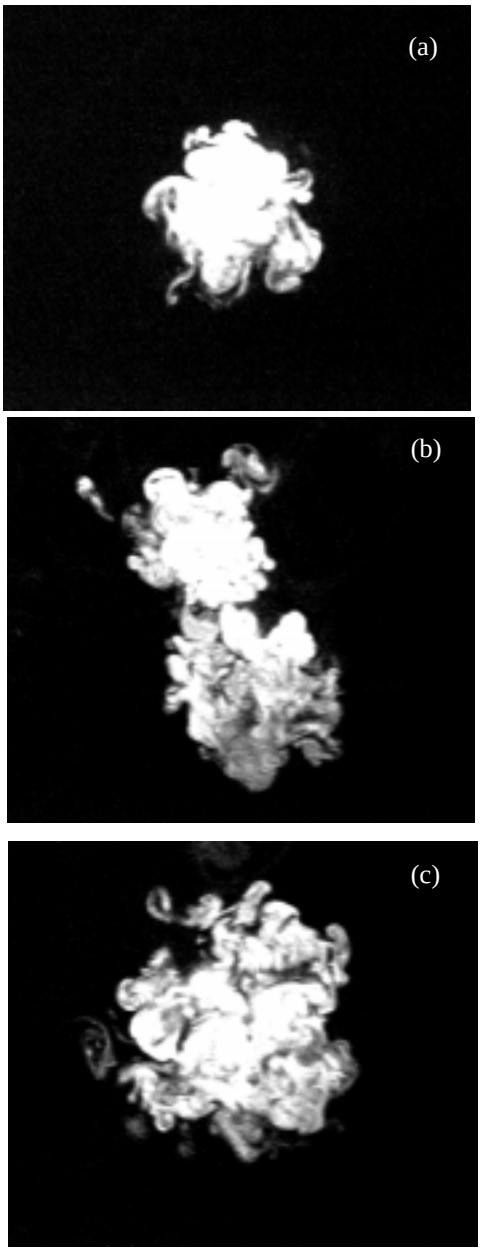

Fig. 12 Transverse sectional views at x/D=8, (a) natural jet, (b) Bifurcating jet with Alternative Mode control, (c) Spreading jet with Rotary Alternative Mode control.

and bent vortices are shed and transported into two different directions by their mutual interaction. It is noted that this control scheme uses only control input at the nozzle lip without axial forcing. Since most previous studies require the combination of azimuthal and axial forcing [8, 10], the present method is simpler and should be advantageous when introduced to industrial applications.

When the plane of asymmetry of the flap motion in Alternative Mode is rotated by 60 degree by each actuation period (hereafter, Rotary Alternative Mode), the vortex rings are shed successively into six divergent directions as shown in Fig. 11.

Figure 12 show an instantaneous cross-stream views of various jets at x/D=8. Unlike the natural jet (Fig. 12a), the jet controlled with Alternative Mode (also see, Fig. 10) spreads widely into the two vertical directions as shown in Fig. 12(b). With Rotary Alternative Mode (Fig. 12c), dye spreads in all radial directions, indicating that the mixing should be significantly enhanced.

Velocity Measurement

Figure 13 shows the phase-averaged velocities of the jet with Alternative Mode at x/D = 0.25 and r/D = 0.5. The two velocities of $\langle u \rangle$ and $\langle v \rangle$ are the phase-averaged streamwise and radial components, respectively. The velocities and time are made dimensionless with the centerline velocity at the nozzle exit U_0 (= 217 mm/s) and the period of flapping motion of the actuator t_0 (= 0.42 s or St_a = 0.27). The strong radial and streamwise velocities are induced with the downward (wallward) movement of the flap, whilst the inward fluid motion is induced when the flap moves upward.

Figure 14 shows the streamwise distributions of mean and root-mean-square (rms) velocities. The statistics are calculated as ensemble-averages over two minutes (~25000 samples). The streamwise mean velocity U_m of the natural jet is almost constant at x/D < 5, and then decreases gradually. For Alternative

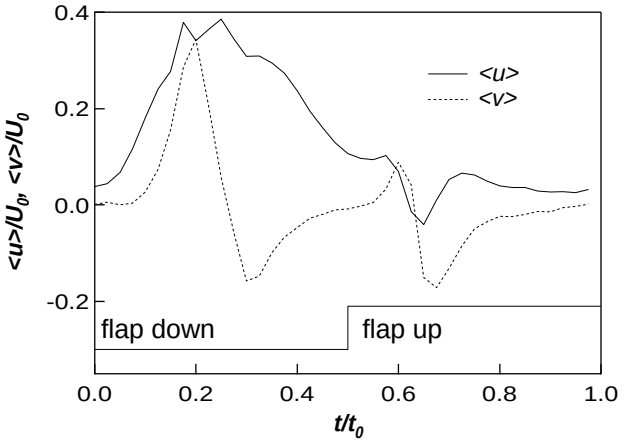

Fig. 13 Phase-averaged streamwise ($\langle u \rangle$) and radial ($\langle v \rangle$) velocities with Alternative Mode control at x/D=0.25 and r/D=0.5.

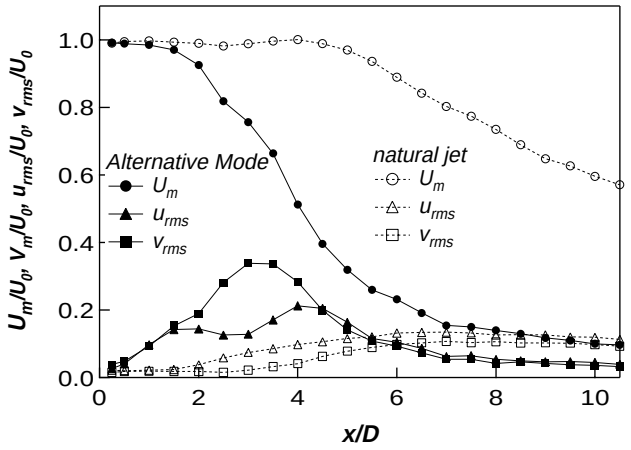

Fig. 14 Streamwise distributions of mean and rms velocities.

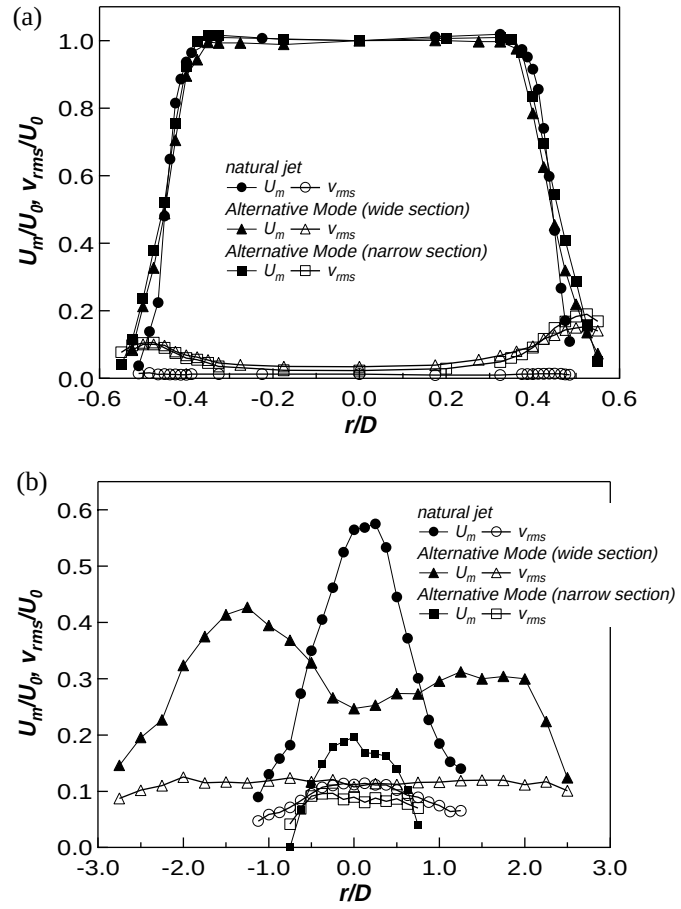

Fig. 15 Radial distributions of U_m and V_{rms}: (a) x/D=0.25, (b) x/D=6.

Mode, however, U_m drops rapidly at $x/D > 2$ and reaches as low as $0.2U_0$ at $x/D > 7$. The rms values of u_{rms} and v_{rms} are markedly increased with their peaks located between x/D = 3 and 4, where the jet bifurcates.

Figure 15(a) shows the radial distributions of U_m and v_{rms} near the nozzle exit (x/D = 0.25). For Alternative Mode, the measurement is made along two cross-flow directions, *i.e.*, in the plane (wide section) and out of the plane (narrow section) of bifurcation. The profiles of U_m are almost the same in all cases, while v_{rms} for Alternative Mode is increased to about 0.1 U_0 in the shear layer. Figure 15(b) shows the distributions at x/D = 6. The profile of U_m in the wide section exhibits two separate peaks and a trough at the centerline, and this fact is consistent with the flow visualization results. On the other hand, U_m in the narrow section has a width smaller than that of the natural jet, and the peak value itself is much smaller. The enhancement of v_{rms} for Alternative Mode over a wide radial range implies that the entrainment of ambient fluid is also increased significantly.

To clarify the relevant conditions of St_a and Re_D for jet bifurcation with Alternative Mode control, the mean centerline velocity at x/D = 6 is measured with hot-film anemometry. Figure 16 shows the contours of the centerline velocity normalized by that of the natural jet under various conditions of St_a and Re_D. It is found that the centerline velocity is decelerated to as much as 55 - 80 % with the optimum flapping frequency of St_a ~0.25 at Re_D <13000.

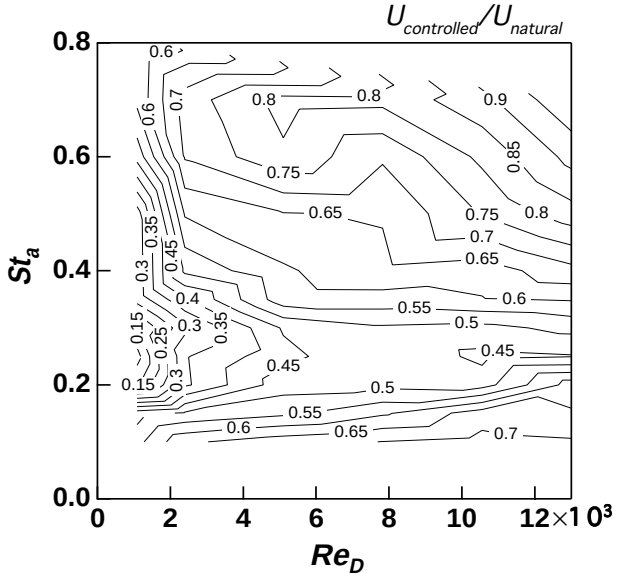

Fig. 16 Relative centerline velocity of the jet controlled at various flapping frequency.

Power Consumption

Since the measured electric resistance of the flap is about 0.01 Ω, the power consumption is roughly estimated to be 0.01W, when 1 A current is applied. The mechanical power input to the ambient fluid by the flap P_f is given as $F_R A_a f$, where A_a and f are the amplitude and frequency of the flap motion, respectively. If the fluid force is assumed to be proportional to the square of the flapping velocity referring to the numerical simulation mentioned before, P_f is estimated to be 6.1×10^{-6} W and 1.6×10^{-5} W in air and water, respectively, at each resonant frequency. This means that the most of the electric energy input is consumed as heat and internal dumping of the flap. Thus, the resultant efficiency of the flap actuator itself is very low, *i.e.*, on the order of 10^{-3} ~ 10^{-4}.

On the other hand, the propulsive power of a jet is given as $P_p = \rho_w U_b^3/2(\pi D^2/4)$, where ρ_w is the density of water, and it is calculated as $P_p = 2.58 \times 10^{-4}$ W in the present experiment. Since the total mechanical energy input by the eighteen flaps is estimated as $P_f = 6.7 \times 10^{-6}$ W when Alternative Mode at 1.6 Hz is applied, the ratio of P_p/P_f reaches about 40. In this case, the static electromagnetic force F given by Eq. (2) with a maximum deflection Δy of 0.4mm is substituted into F_R. Thus, it is concluded that the present control scheme should be very effective.

Moreover, it is likely that the ratio P_p/P_f would be independent of the nozzle size or the flow velocity. If F_R is assumed to be proportional to $SA_a^2 f^2$ with S being the surface area of the flap, then P_f is proportional to $SA_a^3 St_a^{-3} U_b^3/D^3$. This leads to a relation of $P_p/P_f = C(D^2/S)(D/A_a)^3$, provided that St_a is constant. Therefore, the kinetic energy input to the system can be kept small if compared to the energy flux of the system over a wide range of Reynolds number, when the geometric ratios D^2/S and D/A_a are constant.

CONCLUDING REMARKS

The electromagnetic flap actuators for active jet control is designed and fabricated through simple photolithography of a copper plated polyimide film. The static and dynamic responses of the flap are estimated reasonably well with a composite beam model. Those eighteen actuators are mounted on the circular lip of an axisymmetric jet nozzle to control the coherent vortical structures. It is found that these structures are shed being phase-locked to the flap movement and hence the flow field is modified significantly. In particular, when each half cluster of the flaps are driven 180 degree out of phase (Alternative Mode), the jet bifurcates into two separating jets and the centerline velocity drops to about 45 % of that of the natural jet at $x/D = 6$. The most effective Strauhal number is found to be around 0.25 when the Reynolds number is less than 13000.

The present control scheme is very effective, since it requires only a small amount of control input, *i.e.*, about a few percent of the energy flux of the system. However, the dissipative energy loss in the coil of the actuator is unfavorably large, even though the absolute amount of energy consumption (presently, 0.18 W) is not unacceptably large. Thus, the future work should address more efficient actuators for real applications.

ACKNOWLEDGMENTS

The authors gratefully acknowledge Professors H. Miura and I. Shimoyama for their guidance in developing the actuators. We also thank Professor T. Yasuda, Mr. N. Miki, and Ms. H. Inaba for their assistance in the fabrication of the actuators. This work was supported by Ministry of Education, Science, Culture and Sports through the Grant-in-Aid for Scientific Research (No. 10355010).

REFERENCES

[1] Ho, C.-M., and Tai, Y.-C., 1996, "Review: MEMS and Its Applications for Flow Control," *ASME J. Fluids Eng*., **118**, pp. 437-447.

[2] Kasagi, N., 1998, "Progress in Direct Numerical Simulation of Turbulent Transport and Its Control," *Int. J. Heat Fluid Flow*, **19**, pp. 125-134.

[3] Moin, P., and Bewley, T., 1994, "Feedback Control of Turbulence," *Appl. Mech. Rev.*, **47**, pp. S3-S13.

[4] Liu, C. et al., "Out-of Plane Permalloy Magnetic Actuators for Delta-Wing Control," *IEEE MEMS Workshop Proceedings*, Amsterdam, (1995), 7.

[5] Smith, B. L. and Glezer, A., "Vectoring and Small Scale Motions Effected in Free Shear Flows Using Synthetic Jet Actuators," *AIAA-paper*, 97-0213, (1997).

[6] Huang, C. et al., "A Microactuator System for the Study and Control of Screech in High Speed Jets," *IEEE MEMS Workshop Proceedings*, San Diego, (1996), 19.

[7] Bradbury, L. J. S. and Khadem, A. H., "The Distortion of a Jet by Tabs," *J. Fluid Mech*., **70**, (1975), 51.

[8] Lee, M. and Reynolds, W. C., "Bifurcating and Blooming Jets," *Report TF-22, Thermosciences Division, Dept. of Mech. Eng., Stanford University*, (1985).

[9] Crow, S. C. and Champagne, F. H., "Orderly Structure in jet turbulence," *J. Fluid Mech.*, **48**, (1971), 547.

[10] Longmire, E. K. and Duong, L. H., "Bifurcating Jets Generated with Stepped and Sawtooth Nozzles," *Phys. Fluids*, **8**, (1996), 978.